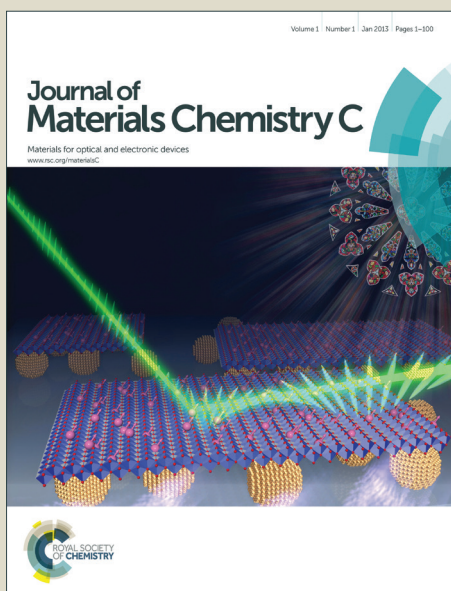


Journal of Materials Chemistry C

Accepted Manuscript



This is an *Accepted Manuscript*, which has been through the Royal Society of Chemistry peer review process and has been accepted for publication.

Accepted Manuscripts are published online shortly after acceptance, before technical editing, formatting and proof reading. Using this free service, authors can make their results available to the community, in citable form, before we publish the edited article. We will replace this *Accepted Manuscript* with the edited and formatted *Advance Article* as soon as it is available.

You can find more information about *Accepted Manuscripts* in the [Information for Authors](#).

Please note that technical editing may introduce minor changes to the text and/or graphics, which may alter content. The journal's standard [Terms & Conditions](#) and the [Ethical guidelines](#) still apply. In no event shall the Royal Society of Chemistry be held responsible for any errors or omissions in this *Accepted Manuscript* or any consequences arising from the use of any information it contains.



www.rsc.org/materialsC

Investigation on preparation and electric field tunable dielectric properties of novel bismuth magnesium niobate transparent capacitors for opto-electronic devices

Shihui Yu, Lingxia Li*, Dan Xu, Heilei Dong, Yuxin Jin

School of Electronic and Information Engineering, Tianjin University, Tianjin 300072,

P. R. China

Abstract

Transparent capacitors, based on the bismuth magnesium niobate ($\text{Bi}_{1.5}\text{MgNb}_{1.5}\text{O}_7$, BMN), have been fabricated on indium tin oxide glass substrates by rf magnetron sputtering. The effect of the post-annealing condition on structural, electrical, and optical properties of BMN thin films was investigated. X-ray diffraction patterns and scanning electron microscopy reveal that the BMN thin films post-annealed in the oxygen partial pressure of 0.1 MPa have the best crystalline quality of all the post-annealing condition. The BMN thin films exhibit an average transmittance of 85% in the visible light range (380-780 nm), while the value of optical absorption edge is 3.59 eV. Dielectric measurements indicate that the thin films exhibit medium dielectric constant of about 99, low loss tangent of 0.0037, and superior tunable dielectric properties at room temperature. Calculations of dielectric tunability and figure of merit (FOM) display a maximum value of 28% at 1.3 MV/cm and ~57, respectively. The results show that BMN thin films have great potential for

* Corresponding author: Tel./fax: +86 2227402838.
E-mail address: lingxiali@126.com (L. Li).

electric field tunable transparent capacitors.

Keywords: Thin films; Sputtering; X-ray diffraction; Electrical properties

1. Introduction

In recent years, much attention has been devoted to the development of tunable dielectric materials for electric field controlled, frequency-agile phase shifters and filters operating in the microwave regime [1-4]. $\text{Ba}_x\text{Sr}_{1-x}\text{TiO}_3$ (BST) thin films have been intensively investigated for its large tunability [5, 6]. However, high dielectric loss in the microwave region strongly inhibits their industrial applications [7, 8]. Alternative tunable materials are therefore of great technological and scientific interest [8]. Bismuth-based pyrochlores have been found to be of interest for low-fired high frequency dielectric application because of their low dielectric loss, low leakage current density, good temperature stability, medium dielectric constant and electric-field tunability [9-11]. Among these, the $\text{Bi}_2\text{O}_3\text{-MgO-Nb}_2\text{O}_5$ system is attracting more attention as microwave tunable dielectric mainly due to its very low dielectric loss and moderate dielectric constant [12, 13]. In addition, the cubic pyrochlore $\text{Bi}_{1.5}\text{MgNb}_{1.5}\text{O}_7$ (BMN) thin films are reported to demonstrate large electric-field tunability of ~39% achieved at a maximum applied bias field of 1.6 MV/cm [8].

Recently, there are several studies on fabricating transparent dielectric oxide devices based on transparent conducting glasses [14, 15]. Moreover, combining an

optically transparent substrate with wide band gap oxides to form thin film transistors gives interesting opportunities for optical applications [16, 17]. In such applications, the dielectric layer with a high dielectric constant is very effective in realizing thin film devices with a low driving bias field. BMN has been posited to have suitable properties for such device applications [8]. Additionally, the integration of high dielectric constant ceramic films on transparent conductive oxide (TCO) films with glass substrate increases the freedom of design of novel photovoltaic devices.

There are numerous deposition techniques used to grow dielectric oxide thin films including molecular beam epitaxy (MBE) [1, 18], sol-gel processing [2, 3, 11, 19], magnetron sputtering [5, 8], metal-organic chemical vapor deposition (MOCVD) [20], chemical solution deposition (CSD) [21, 22] and pulsed laser deposition (PLD) [10, 23]. Among fabrication methods, magnetron sputtering is considered to be the most favorable deposition method to obtain highly uniform films even on polycrystalline substrates at high deposition rates. Also, the surface of the thin films grown by magnetron sputtering can be very smooth [4]. The thin films with smooth surface are advantages for transparent dielectric oxide devices.

It is worth noting that indium tin oxide (ITO glass) is a low cost and an industrialized substrate [24], herein BMN thin films were deposited on the ITO glass substrates by magnetron sputtering. The post-annealing process after thin film deposition is considered to be an effective way to improve the quality of thin film [25]. Therefore, an investigation of post-annealing of BMN thin films is considered to be valuable. In this paper, the transparent capacitors based on the BMN thin films were

deposited on the ITO glass substrates at 500 °C by magnetron sputtering. The influences of post-annealing on the crystallinity, surface topography, optical and electrical properties of BMN thin films have been systematically investigated

2. Experimental

The $\text{Bi}_{1.5}\text{MgNb}_{1.5}\text{O}_7$ ceramic target was prepared by solid state reaction process with Bi_2O_3 , MgO , and Nb_2O_5 as starting materials. The mixtures of starting materials in stoichiometry were pressed into 3 inch diameter and 4 mm thickness pellet at 20 tons and then sintered at 1180 °C for 4h in air. The ITO glass substrates were cleaned in an ultrasonic bath with alcohol for 30 min. BMN thin films were deposited on ITO glass substrates by rf magnetron sputtering from the BMN ceramic target. The target to substrate distance was kept as 10 cm. Before sputtering, the vacuum chamber was evacuated down to a base pressure of 7.0×10^{-6} Torr. High purity (99.99%) Ar and (99.99%) O_2 were introduced through separate mass flow controllers. The total pressure during sputtering was maintained at 10 mTorr, and the O_2/Ar ratio was 3:17. The substrate temperature was controlled at 500 °C. The depositing power was fixed at 150 W. Before deposition, the target was pre-sputtered in O_2+Ar atmosphere for 15 min to remove any impurity on the surface of the target. The film thickness was controlled to be ~220 nm. After the deposition, thin films were annealed at 700 °C for 10 min in air, oxygen partial pressure of 0.02 MPa and oxygen partial pressure of 0.1 MPa, respectively. In the end, Au top electrodes with 0.2 mm in diameter were patterned by lift-off process to prepare the capacitor.

The crystallinity was determined by X-ray diffraction using a (Rigaku

D/MAX-RB, Akishima, Tokyo, Japan) system equipped with a Cu-K α radiation source (1.542 Å) scanning the diffraction angles (2θ) between 20° and 70° (increment 0.02°). Thin film morphologies were investigated by scanning electron microscopy (JEOL JSM-7600F, Akishima, Tokyo, Japan). The thickness of the films was measured by Alpha-Step D-100 profilometer (KLA-Tencor, California, USA). For electrical measurement, Au top electrodes with 0.2 mm in diameter were patterned by lift-off process to form the metal-insulator-metal type capacitors. The dielectric properties, tunability were measured at room temperature by Aglient 4285A precision LCR meter (Santa Clara, California, USA). The leakage current of the films was measured by Aglient 4339B High Resistance Meter (Santa Clara, CA, USA) at room temperature. And the optical transmittance spectra were obtained on an ultraviolet-visible-near infrared (UV-Vis-NIR) spectrophotometer (Cary 5000, Varian).

3. Results and discussion

Fig. 1 displays the XRD patterns of the BMN thin films grown on the ITO glass substrates with different post-annealing methods. The as-deposited BMN thin films are amorphous in nature when deposited at 500 °C without post-annealing. However, the thin films begin to crystallize when post-annealed at 700 °C. After the deposition of thin film is completed, the adatoms and ions on the substrate cannot get enough energy to migrate, resulting in the thin films are amorphous. After post-annealing, the adatoms and ions get the follow-up energy from the post-annealing process to overcome the barrier and reach their ideal position [26]. The crystal growth is

governed by the principle of minimum energy and the annealing process easily makes the crystal being in the minimum energy state [27, 28]. As shown in Fig.1, all thin films post-annealed at 700 °C exhibit cubic pyrochlore phase structure. No other phase can be detected in the XRD patterns except of the character peaks of ITO/grass substrate. The (2 2 2) peak intensity initially increases with increasing oxygen partial pressure. These phenomena can be explained as follows. For BMN thin films post-annealed in the air, there exist lots of oxygen vacancies, thus resulting in the fact that the chemical composition of BMN thin films is non-stoichiometric and then the BMN thin films have worse crystalline. There are still many oxygen vacancies in the BMN thin film, when annealed in oxygen partial pressure of 0.02 MPa. However, the post-annealing in oxygen partial pressure of 0.1 Mpa is much more effective to the reducing or elimination of oxygen vacancies, and the crystalline become better, therefore, the (2 2 2) peak intensity increase.

The SEM images of the surfaces of BMN thin films s grown on the ITO glass substrates with different post-annealing methods are presented in Fig. 2a-d. When the BMN thin films deposited at 500 °C without the post-annealing treatment, the film did not crystallize, the surface is inhomogeneous and incompact, as shown in Fig. 2a). After post-annealed at 700 °C (Fig. 2 b-d), it is clear that by post-annealing treatment, the grain was refined, the surface of the films became more homogeneous and dense. As we know that the grain size is controlled by the two progresses, namely, nucleation and growth in the films. When in the relative low grown temperature, the interfacial energy of the films is high. It is difficult to crystallize the thin films (Fig. 2a). By

post-annealing at 700 °C in air, these zones of un-crystallization will be crystallization, especially in the surface of the films. The interfacial energy becomes lower in the post-annealing method, a great amount of the nucleus site of the films will greatly increase, and the films are well crystallized, naturally, fine grains are attainable. These grains will grow in the following oxygen partial pressure, and then we can gain the grains with much bigger grain size and better crystalline quality (Fig. 2d). The above SEM results are consistent with the XRD results.

The spectral transmission curves of the BMN thin films grown on the ITO glass substrates with different post-annealing methods are shown in Fig. 3a. All the transmission spectra show interference fringes which originate due to interference at the air and substrate thin film interfaces (As shown in Fig. 2). The sharp fall in transmission and disappearance of the fringes at the shorter wavelength is due to the fundamental absorption of the thin films. Average transmittance of BMN thin film can be defined as follows [29]:

$$T_{av} = \frac{\int V(\lambda)T(\lambda)d\lambda}{\int V(\lambda)d\lambda} \quad (1)$$

where $T(\lambda)$ is the measured transmittance of thin film system, and $V(\lambda)$ is the photopic luminous efficiency function defining the standard observer for photometry. The range of λ is from 380 nm to 780 nm. $V(\lambda)$ approaches zero beyond this region and reaches the maximum of 1 at 555 nm, the medium of this region. The optical transmittance of as-deposited BMN thin films deposited at 500 °C without post-annealing is about 70% in the visible range of wavelengths (380-780 nm). After post-annealing, we can see that all the BMN thin films show high transmittance

(above 80%) in the visible region. The average optical transmittance values are 80%, 84%, and 86% for the BMN thin films post-annealed in the air, post-annealed in oxygen partial pressure of 0.02 MPa and post-annealed in oxygen partial pressure of 0.1 MPa, respectively. It is observed that the average optical transmittance increases with the increase in the oxygen partial pressure. The optical transmission of thin film is strongly depending on its structure, surface morphology and density. The increase of the optical transmittance of BMN thin film with the increase of oxygen pressure can be attributed to a weakening of the scattering, and the absorption of light, due to the increase of the crystallinity. In addition, since surface state is related to deep level defects, which are most probably due to oxygen vacancies or bismuth interstitials, the surface state level will absorb visible photons [30]. But the surface state density of the BMN thin film greatly decreases with increasing oxygen partial pressure (as shown in Fig. 2), therefore, the optical transmittance increases.

The transmittance data obtained for the film is used to calculate the absorption coefficients at different wavelengths using the following relation [31]:

$$\alpha = \frac{\ln(1/T)}{d} \quad (2)$$

where d is the film thickness, α is the absorption coefficient and T is the transmittance of the thin film. The fundamental absorption, which corresponds to the electron excitation from valance band to conduction band, is usually used to determine the value of optical band gap (E_g) using the Tauc relationship [32],

$$a \propto C(h\nu - E_g)^n \quad (3)$$

where C is a constant, ν is the transition frequency and the exponent n characterizes

the nature of band transition. $n = 1/2$ and $3/2$ corresponds to direct allowed and direct forbidden transitions and $n = 2$ and 3 corresponds to indirect allowed and indirect forbidden transitions, respectively [33]. Inter-band optical transitions that can be described by wave functions localized over a distance of the order of lattice constant are relatively unchanged by disorder. Therefore, optical band gap and the constant C estimated from $\alpha^{1/n}$ vs E reflects its local atomic structure undetected by XRD. That is, these parameters can be correlated with the short-range order at the nano-scale and, particularly, amorphous phase alone or phases co-existing with crystalline materials in films. It is observed that for all the films, the best straight line is obtained for $n = 1/2$ which is expected for direct allowed transitions. The optical band gap of as-deposited BMN thin film without post-annealing obtained from Fig. 3b is 3.45 eV. After post-annealing, the optical band gaps for the BMN thin films post-annealed in the air, post-annealed in oxygen partial pressure of 0.02 MPa and post-annealed in oxygen partial pressure of 0.1 MPa, are 3.52, 3.56 and 3.59 eV, respectively. The optical band gap also shows an increase on oxygen partial pressure, indicating the decrease of amorphous state and the defect in the BMN thin film. The low band gap in the as-deposited thin films may be due to the disorder crystalline structure and too much defect the increase in optical band gap what reflects the crystallinity in the BMN thin films.

The dielectric constant and dielectric loss were measured by applying a small ac signal of 0.5 V amplitude as a function of frequency in the range of 75 kHz–30 MHz. Fig. 4a gives the frequency dependence on the dielectric constant and dielectric loss

of the BMN thin films with different post-annealing methods. It can be seen that there is little or no dispersion of dielectric constant in the frequency range from 0.075 MHz to 30 MHz for all the BMN thin films. This type of result ruled out the presence of the effect of mobile charges in the film, which may accumulate near the top and bottom interface between the film and electrode [7]. At frequency >4 MHz, though the dielectric constants remain constant, the loss tangents slightly increase with frequency. Such increase in loss tangents accompanied by a constant value of dielectric constant should be attributed to resonance effect. The resonance may arise due to the matching of the frequency of charge transfer between the cations and anions, and that of the applied electric field [34]. In addition, a similar inference can also be drawn from frequency dependence dielectric loss curves.

The dependence of the dielectric constant and the loss tangent of BMN thin films with different post-annealing methods at a measuring frequency of 1 MHz is shown in Fig. 4b. For the as-deposited thin film, the dielectric constant value is ~ 52 at 1 MHz, measured at room temperature. After post-annealing, the dielectric properties of BMN thin films show the obvious improvement. Dielectric constant increases and loss tangent decreases. The dielectric constant of the BMN thin films grown on ITO glass post-annealed in air, post-annealed in oxygen partial pressure of 0.02 MPa and post-annealed in oxygen partial pressure of 0.1 MPa, was 81, 93 and 99, respectively, measured at a frequency of 1 MHz and at room temperature. This difference in dielectric properties in these three kinds of BMN thin films may be attributed due to different grain size and change in the direction and magnitude of electric polarization

in orientation engineered BMN thin films [35]. These polarization changes come from the magnitude variation of the relative displacement of the Nb ion with respect to the O ion, the domain crystallize mechanism change, and the strain and stress changes in perovskite BMN thin film [36]. The room temperature dielectric constant of the BMN thin films post-annealed in oxygen partial pressure of 0.1 MPa is relatively higher than that of the thin films post-annealed in oxygen partial pressure of 0.02 MPa and post-annealed in air. The enhancement of the dielectric constant was attributed to the relatively larger grain size of the BMN thin film with (222) orientation (As shown in Fig. 1 and Fig. 2). The high loss tangent observed for the as-deposited BMN thin film, the decrease in loss tangent of thin films post-annealed at 700 °C may be attributed to the low leakage current because of decrease of defects in the thin film and the crystal of the thin films. The thin films post-annealed in oxygen partial pressure of 0.1 MPa show loss tangent as low as 0.0037 at 1 MHz.

The bias-field dependence of the dielectric constant and the loss tangent at 1 MHz for BMN thin films deposited on ITO glass substrates with different post-annealing methods are shown in Figs. 4c. Defining the dielectric tunability in bias field as $[\epsilon(0)-\epsilon(v)]/\epsilon(0)$, where $\epsilon(0)$ is the measured dielectric constant at zero bias field and $\epsilon(v)$ is the dielectric constant at the maximum applied bias field [8, 37]. According to Fig. 4d, the as-deposited BMN thin film exhibits the lowest dielectric tunability of 7% at a bias field of 1.3 MV/cm. After post-annealing, BMN thin films exhibit the excellent dielectric tunability. The tunability of the BMN thin film post-annealed in air is 19% (1.8 MV/cm) and the tunability of the film post-annealed

in oxygen partial pressure of 0.02 MPa is 24% (1.8 MV/cm), whereas that of the BMN thin film post-annealed in oxygen partial pressure of 0.1 MPa reaches 28% at 1.8 MV/cm. The tangent of BMN thin film post-annealed in oxygen partial pressure of 0.1 MPa is about 0.004, changing little with the downward and upward bias fields. After post-annealing, with the increase of oxygen partial pressure, the increase in tunability is probably because a different microstructure and less oxygen vacancies and defects in the BMN thin films, which in turn affects the tunability of the thin films [38].

In electrically tunable applications, the figure of merit (FOM) is usually used to evaluate the quality of tunable materials. The FOM is defined as [39, 40].

$$\text{FOM} = \frac{\text{tunability}}{\tan \delta} \quad (4)$$

Fig. 4d shows the FOM as a function of electric field for the BMN thin films. As shown in Fig. 4d, the as-deposited BMN thin film has a FOM of 7 at 1.3 V/cm, the thin film post-annealed in air has a FOM of 41 at 1.8 MV/cm, the post-annealed in oxygen partial pressure of 0.02 MPa has a FOM of 48 at 1.8 MV/cm, and the post-annealed in oxygen partial pressure of 0.1MPa has a maximum FOM of 57 at 1.8 MV/cm. The high FOM values can attribute to the excellent tunability and the lower dielectric loss.

As shown in Fig. 5, the BMN thin films post-annealed in oxygen partial pressure of 0.1MPa have significantly lower loss tangent in the all samples. The factors influencing the dielectric loss are quite complicated. However, at low frequency considered in this study, the overall dielectric loss is dedicated by the polarization loss

(it is strongly affected by space dipole determined by interface conditions and defects in BMN thin films) and leakage conductance loss. The leakage conductance loss was evaluated by leakage current measurements. The relationship between leakage current density and applied bias field for BMN thin films are shown in Fig. 5. The as-deposited BMN thin films deposited on ITO glass substrate shows the highest leakage current density ($8.0 \times 10^{-4} \text{ A/cm}^2$) at the applied field of 0.45 MV/cm . After post-annealing, the leakage current density decrease evidently ($< 5.0 \times 10^{-5} \text{ A/cm}^2$), compared to the as-deposited BMN thin films. However, with the oxygen partial pressure increasing, the leakage current density increase density of thin films post-annealed increases slight. We believe that microstructure, grain size, grain boundary all play certain roles in the leakage current behavior of these thin films. This can be explained as follows. There are lots of deficient sites in the as-deposited BMN thin films without post-annealing, because the BMN thin film is amorphous, therefore, the leakage current density is very high. After post-annealing, the grain sizes of thin films increase as the increase of oxygen partial pressure, as shown in Fig. 2, the BMN thin films with larger grain sizes and more aligned grain configurations have overall shorter conduction paths along the grain boundaries, which causes an increase slight in the leakage current density.

4. Conclusions

We have fabricated novel $\text{Bi}_{1.5}\text{MgNb}_{1.5}\text{O}_7$ transparent capacitors using rf magnetron sputtering technique. The structural, microwave dielectric and optical properties of $\text{Bi}_{1.5}\text{MgNb}_{1.5}\text{O}_7$ thin films grown on ITO glass substrates were

investigated to verify the influences of post-annealing process. The oxygen partial pressure dependence of the optical transmittance, band gap and dielectric properties of these thin films were studied both in amorphous and crystalline forms. X-ray diffraction patterns and scanning electron microscope analysis reveal that the BMN thin film post-annealed in the oxygen partial pressure of 0.1 MPa had the best crystalline quality. The BMN thin film post-annealed in the oxygen partial pressure of 0.1 MPa showed the best dielectric properties, with a dielectric constant of 99 at 1 MHz, dielectric tunability of 28%, dielectric loss of 0.0037, and a mean optical transmittance in visible wavelength of 85% in the visible wavelength regions with an optical absorption edge value of 3.59 eV. Moreover, the relatively low leakage current associated with post-annealing at 700 °C enables these novel $\text{Bi}_{1.5}\text{MgNb}_{1.5}\text{O}_7$ transparent capacitors to be integrated into opto-electronic devices.

Acknowledgments

This work was supported financially by Program for New Century Excellent Talents in University (NCET), 863 Program (2007AA03Z423) and China Postdoctoral Science Foundation.

References

- [1] M. Evgeny, P. K. Adam, J. H. Adam and S. Susanne, *Appl. Phys. Lett.*, 2012, **101**, 252906.
- [2] X. Sun, Y. Yang, Q. Zhang, S. Hou, C. Huang, Z. Hu, J. Zou, M. Li, T. Peng and X. Zhao, *J. Am. Ceram. Soc.*, 2013, **96**, 820.

- [3] S. Chao, B. Ma, S. Liu, M. Narayanan and U. Balachandran, *Mater. Res. Bull.*, 2012, **47**, 907.
- [4] K. Li, X. Dong, D. Rémiens, X. Lei, T. Li, G. Du and G. Wang, *J. Am. Ceram. Soc.*, 2013, **96**, 1682.
- [5] Z. Feng, W. Chen, and O. K. Tan, *Mater. Res. Bull.*, 2009, **44**, 1709.
- [6] J. Liao, Z. Xu, X. Wei, X. B. Wei, P. Wang and B. Yang, *Surf. Coat. Tech.*, 2012, **206**, 4518.
- [7] L. B. Kong, S. Li, T. S. Zhang, J. W. Zhai, F. Y. C. Boey and J. Ma, *Prog. Mater. Sci.*, 2010, **55**, 840.
- [8] S. W. Jiang, Y. R. Li, R. G. Li, N. D. Xiong, L. F. Tan, X. Z. Liu and W. Tao, *Appl. Phys. Lett.*, 2009, **94**, 162908.
- [9] L. Yang, G. Wang, X. Dong and D. Rémiensy, *J. Am. Ceram. Soc.*, 2010, **93**, 1215.
- [10] X. Zhang, W. Ren, P. Shi, X. Wu, X. Chen and X. Yao, *J. Alloys Comds.*, 2013, **553**, 8.
- [11] P. Ning, L. Li, X. Zhang, M. Wang and W. Xia, *Mater. Lett.*, 2012, **87**, 5.
- [12] L. Gao, S. Jiang, R. Li, B. Li and Y. Li, *Thin Solid Films*, 2012, **520**, 6295.
- [13] H. B. Nguyen, L. Norén, Y. Liu, R. L. Withers, X. Wei, and M. Elcom, *J. Solid State Chem.*, 2007, **180**, 2558.
- [14] G. Zhu, H. Xu, Z. Yang and A. Yu, *Thin Solid Films*, 2013, **531**, 415.
- [15] Y. C. Liang, C. L. Huang and C. Y. Hu, *J. Alloys Comps.*, 2011, **509**, 7948.
- [16] M. W. J. Prins, K. O. Grosse-Holz, G. Muller, J. F. M. Cillessen, J. B. Giesbers, R. P. Weening and R. M. Wolf, *Appl. Phys. Lett.*, 1996, **68**, 3650.

- [17] I. Titkov, I. Pronin, L. Delimova, I. Liniichuk and I. Grekhov, *Thin Solid Films*, 2007, **515**, 8748.
- [18] S. Y. Wang, X. Qiu, W. F. Liu, Y. Zhu and D. J. Li, *J. Cryst. Growth*, 2011, **324**, 130.
- [19] B. Ma, S. Tong, M. Narayanan, S. Liu, S. Chao and U. Balachandran, *Mater. Res. Bull.*, 2011, **46**, 1124.
- [20] N. M. Sbrockey, G. S. Tompa, T. S. Kalkur and J. Zhang, *J. Vac. Sci. Tech. B*, 2012, **30**, 061202.
- [21] K. C. Sekhar, K. P. Hong, S. H. Key, C. S. Han, J. C. Kim, D. S. Kim, J. C. Park and Y. S. Cho, *Thin Solid Films*, 2013, **527**, 267.
- [22] X. Tang, X. Zhu, J. Dai and Y. Sun, *Acta Mater.*, 2013, **61**, 1739.
- [23] X. Zhang, W. Ren, X. Zhan, Z. Wang, P. Shi, X. Chen, X. Wu and X. Yao, *Thin Solid Films*, 2012, **520**, 141.
- [24] S. Yu, W. Zhang, L. Li, D. Xu, H. Dong and Y. Jin, *Appl. Surf. Sci.*, 2013, **286**, 417.
- [25] Y. L. Huang, Y. C. Le, D. C. Tsai, J. D. Chiu, and F. S. Shieu, *J. Eur. Ceram. Soc.*, 2013, **33**, 2609.
- [26] X. H. Zhang, W. Ren, P. Shi, X. F. Chen and X. Q. Wu, *Appl. Surf. Sci.*, 2010, **256**, 6607.
- [27] X. H. Zhang, W. Ren, P. Shi, X. F. Chen, and X. Q. Wu, *Appl. Surf. Sci.*, 2010, **256**, 1861.
- [28] S. G. Kim, S. B. Mah, N. W. Jang, D. S. Paik and C. Y. Park, *Mater. Lett.*, 2000,

- 43**, 254.
- [29] S. Yu, W. Zhang, L. Li, D. Xu, H. Dong and Y. Jin, *Acta Mater.*, 2013, **61**, 5429.
- [30] W. Yang, Z. Wu, Z. Liu, A. Pang, Y. L. Tu and Z. C. Feng, *Thin Solid Films*, 2010, **519**, 31.
- [31] J. C. Tauc, *Optical Properties of Solids*. Amsterdam: North-Holland; 1972.
- [32] S. H. Yu, C. H. Jia, H. W. Zheng, L. H. Ding and W. F. Zhang, *Mater. Lett.*, 2012, **85**, 8568.
- [33] A. Masuno, H. Inoue, J. Yu and Y. Arai, *J. Appl. Phys.*, 2010, **108**, 063520.
- [34] K. C. Verma, R. K. Kotnala, M. C. Mathpal, N. Thakur, P. Gautam, and N. S. Negi, *Mater. Chem. Phys.*, 2009, **114**, 576.
- [35] M. Nayak and T. Y. Tseng, *Thin Solid Films*, 2002, **408**, 194.
- [36] S. E. Moon, E. K. Kim, M. H. Kwak, H. C. Ryu, Y. T. Kim, K. Y. Kang and S. J. Lee, *Appl. Phys. Lett.*, 2003, **83**, 2166.
- [37] X. H. Zhu, E. Defaÿ, B. Guigues, G. L. Rhun, C. Dubarry and M. Aid, *J. Eur. Ceram. Soc.*, 2010, **30**, 471.
- [38] J. Wang and T. M. K. Susan, *App. Phys. Lett.*, 2006, **89**, 172906.
- [39] Y. L. Kuo and J. M. Wu, *Appl. Phys. Lett.*, 2006, **89**, 132911.
- [40] L. Yang, G. Wang and X. Dong, *J. Am. Ceram. Soc.*, 2010, **93**, 1215.

Figure captions

Figure 1. X-ray diffraction patterns of BMN thin films grown on the ITO glass substrates with different post-annealing methods (a. ITO glass, b. as-deposited, c. post-annealed in air, d. post-annealed in oxygen partial pressure of 0.02 MPa, e. post-annealed in oxygen partial pressure of 0.1 MPa).

Figure 2. SEM surface morphologies of BMN thin films: (a) as-deposited films, (b) post-annealed in air, (c) post-annealed in oxygen partial pressure of 0.02 MPa and (d) post-annealed in oxygen partial pressure of 0.1 MPa.

Figure 3. (a) The optical transmittance spectra of BMN thin films with the different post-annealing methods; (b) The optical band gap of BMN thin films with the different post-annealing methods. (a. as-deposited films, b. post-annealed in air, c. post-annealed in oxygen partial pressure of 0.02 MPa, d. post-annealed in oxygen partial pressure of 0.1 MPa).

Figure 4. (a) Frequency dependence of the dielectric properties of BMN thin films with the different post-annealing methods; (b) Dependence of dielectric constant and loss tangent at 1 MHz for BMN thin films with the different post-annealing methods; (c) The bias field dependence of the dielectric constant and the loss tangent at 1 MHz for BMN thin films with the different post-annealing methods; (d) The figure of merit of BMN thin films with the different post-annealing methods. (a. as-deposited films, b.

post-annealed in air, c. post-annealed in oxygen partial pressure of 0.02 MPa, d. post-annealed in oxygen partial pressure of 0.1 MPa).

Figure 5. Dc leakage current density vs. applied bias field of BMN thin films with the different post-annealing methods (a. as-deposited films, b. post-annealed in air, c. post-annealed in oxygen partial pressure of 0.02 MPa, d. post-annealed in oxygen partial pressure of 0.1 MPa).

Figures

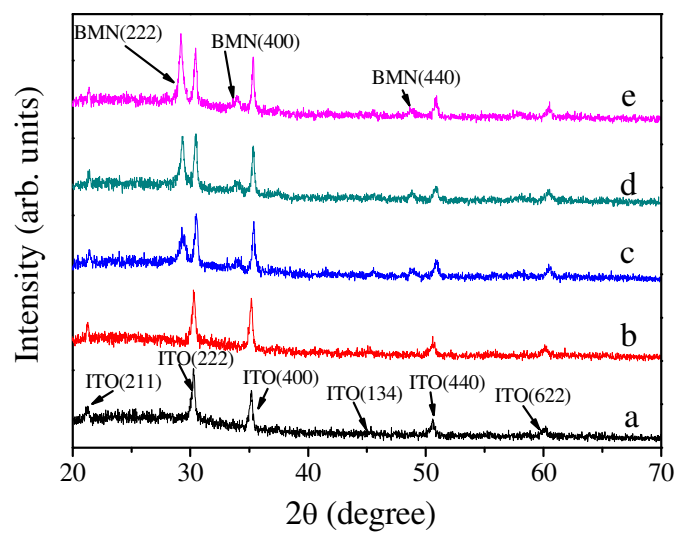


Fig. 1

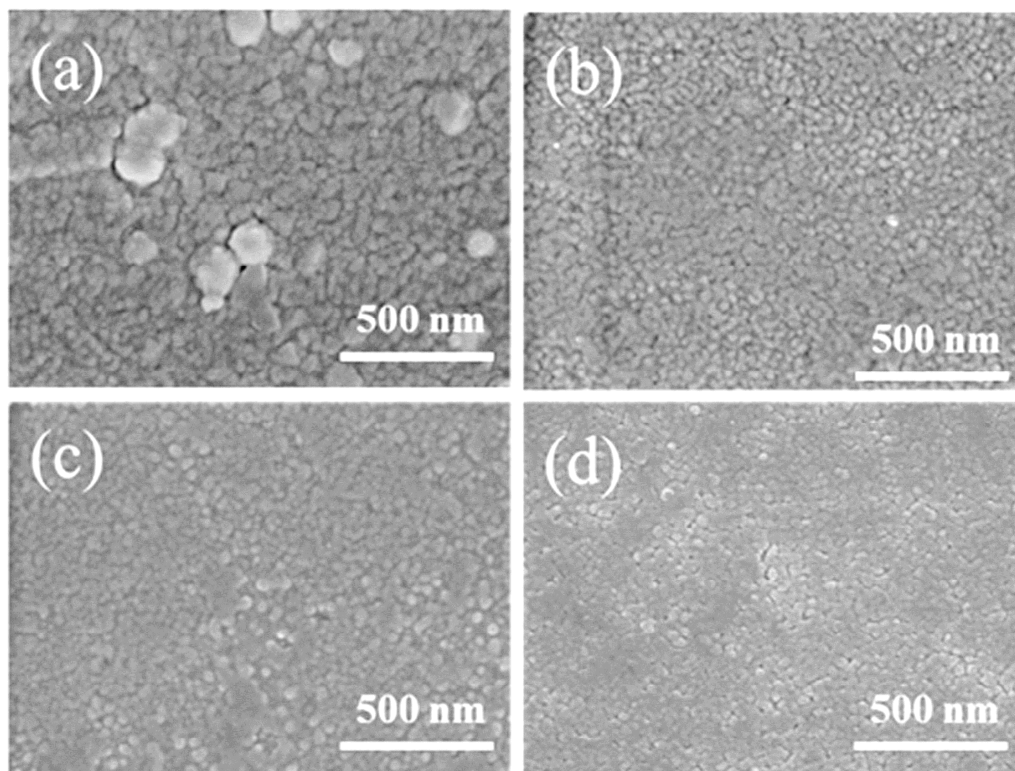


Fig. 2

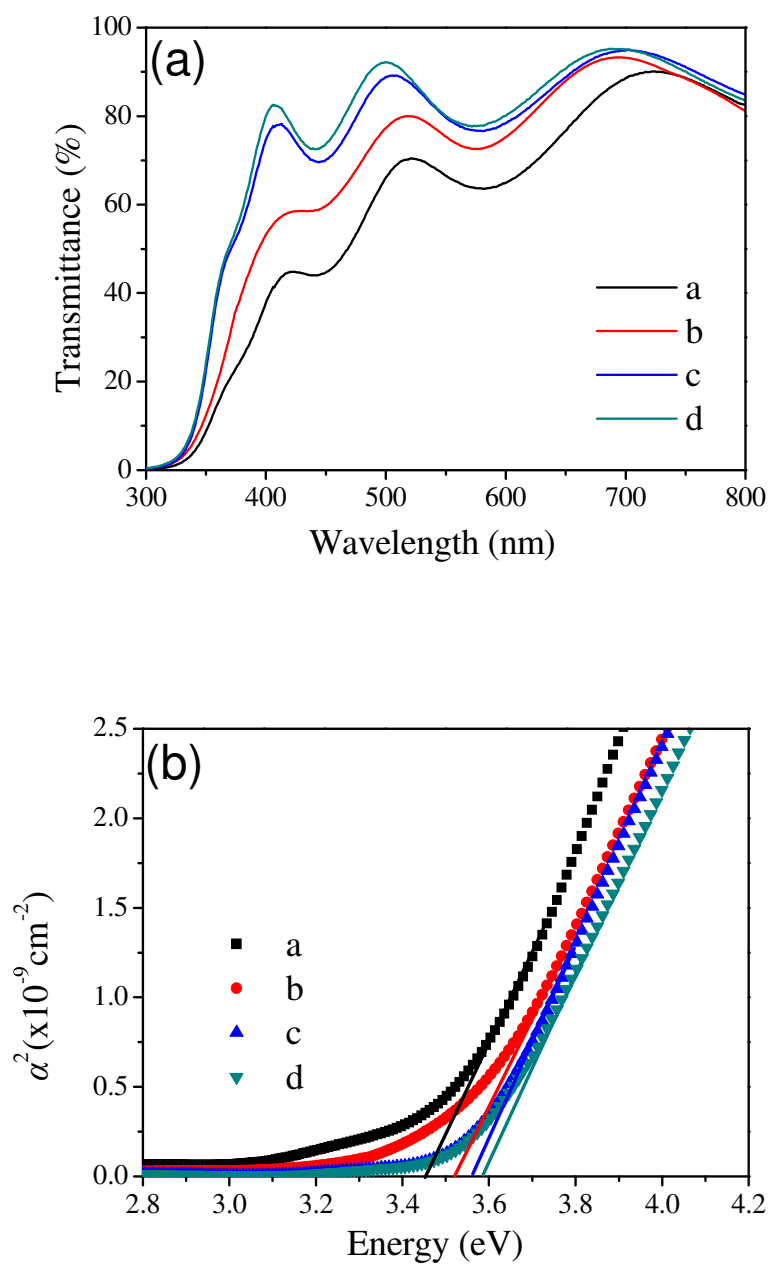
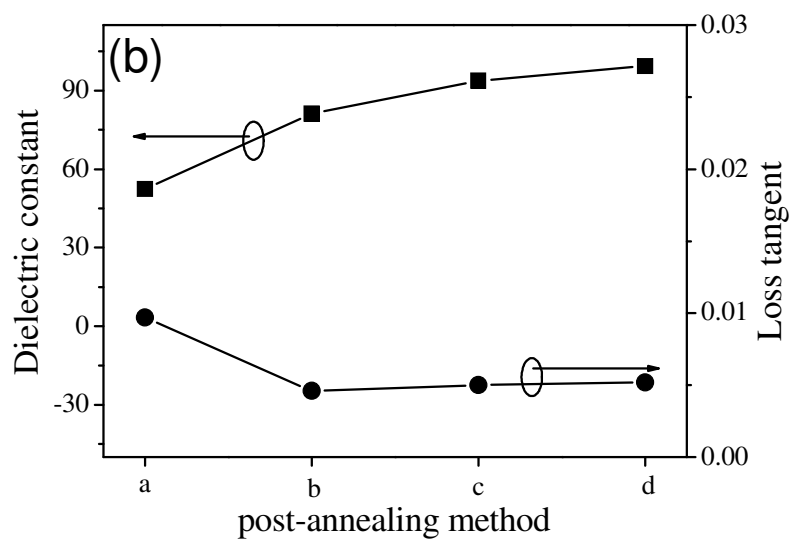
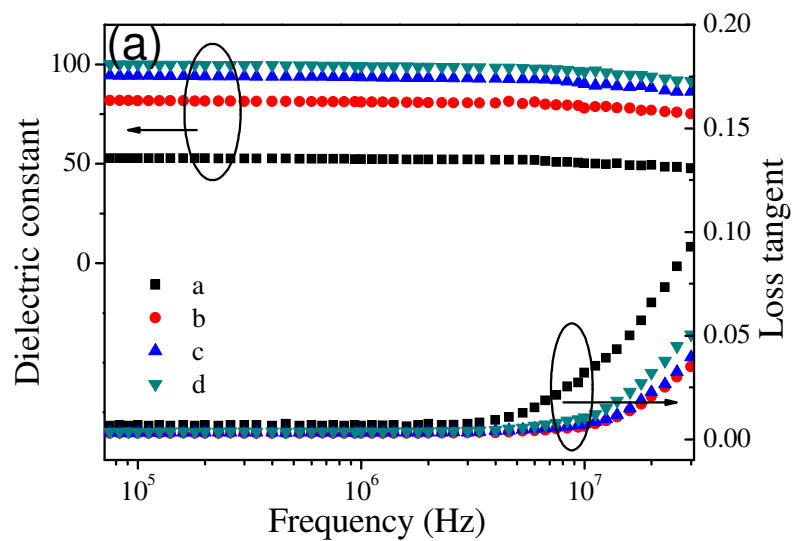


Fig. 3



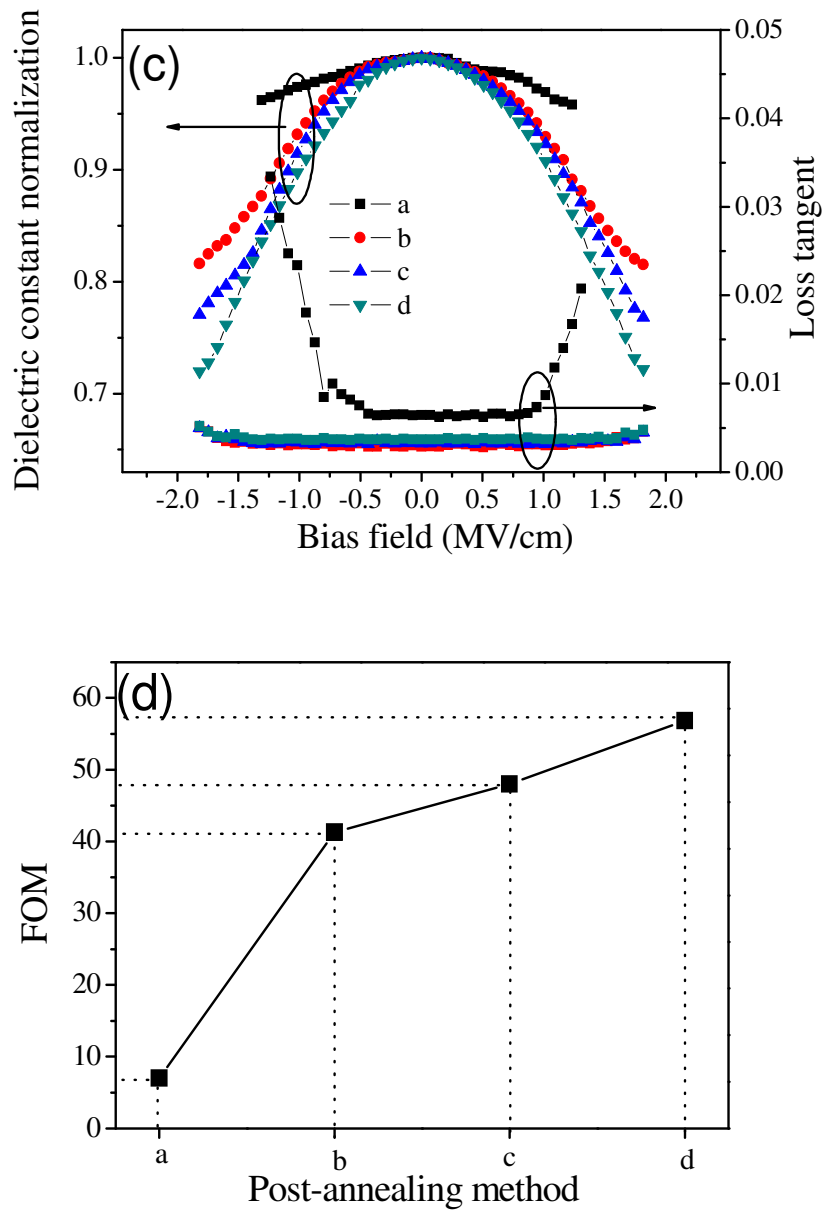


Fig. 4

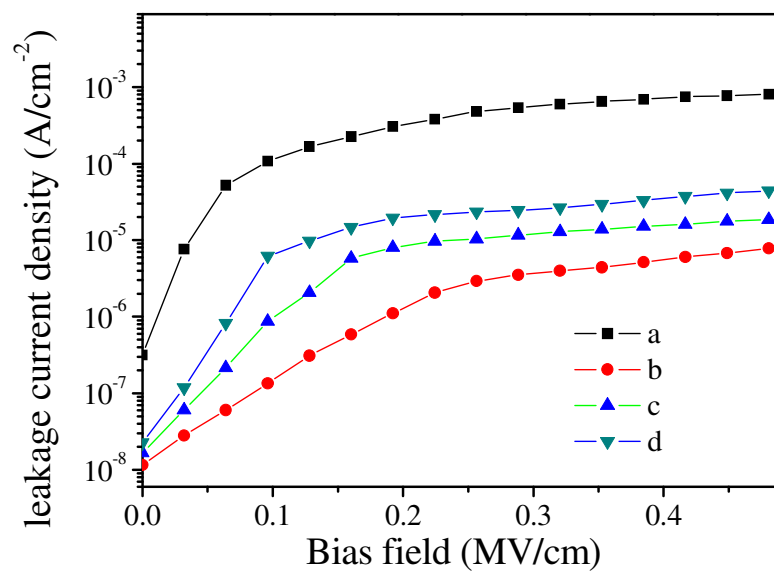


Fig. 5